AIAA JOURNAL
Vol. 44, No. 12, December 2006

Technical Notes

TECHNICAL NOTES are short manuscripts describing new developments or important results of a preliminary nature. These Notes should not exceed 2500 words (where a figure or table counts as 200 words). Following informal review by the Editors, they may be published within a few months of the date of receipt. Style requirements are the same as for regular contributions (see inside back cover).

Optimum Drag Reduction Conditions of Stepped-Nose Objects

Anang Cakrawala* and Akira Umemura†
Nagoya University, Nagoya 464-8603, Japan

DOI: 10.2514/1.23334

I. Introduction

THE flow past a simple square or rectangular object separates at the sharp corners and a large base drag force is exerted by the suction effect arising from the Karman vortices. It is known that an instep cut into each front corner can lead to a significant reduction in the drag force of the object [1,2]. This is because a separation bubble trapped inside the step causes an effective rounding of the corners, allowing the flow to reattach to the side walls of the object, thereby suppressing large-scale separated flow and reducing the base drag force. Furthermore, the pressure drag force on the nose is significantly reduced because the instep vortex produces a low pressure area, creating a net thrust force that partially cancels the drag force. Clearly the level of drag reduction depends on the step size, but the precise nature of this relationship is not yet known. Therefore, to identify the optimum step size and explore its underlying physics, a systematic series of experiments was performed in a wind tunnel.

II. Experimental Method

The test object used in the wind tunnel is shown in Fig. 1. The stepped-nose object was made by inserting a rectangular block into a slot cut in one side of a square base block ($H = 50$ mm in width by 50 mm in length). By changing the size of the base slot and the inserted length of the inserted part, the size of the step was varied. The test object spanned the full width of the wind tunnel test section (450 mm wide and 350 mm high), and was located at a distance of around $5H$ lengths downstream of the wind tunnel's mouth. Its solid blockage was 10%.

For a Reynolds number based on obstacle width $H = 50$ mm and uniform stream velocity $U_\infty = 10$–30 m/s, the experiments were performed in the range from $Re = 0.5 \times 10^5$ to 1.5×10^5. The low-speed wind tunnel used in the experiments has a uniform stream turbulence intensity of around 2%. Three-dimensional effects [3] were present close to the tunnel walls and in the wake region far downstream of the block. However, the changes induced in the flow pattern by the presence of the insteps, which are the principal interest of the present study, were confirmed to occur in a two-dimensional manner over the middle section of the stepped-nose object, where all the measurements were conducted.

Dimensionless variables were introduced: length variables, velocity, and pressure were made dimensionless using the object width H, uniform stream velocity U_∞, and dynamic pressure $\frac{1}{2}\rho U_\infty^2$, respectively. The pressure on the surface of the stepped object was measured by means of pressure transducers, for which purpose orifices 0.5 mm in diameter were drilled into both the base and the inserted nose part. The inclination angle of the orifices relative to the uniform stream direction was varied to minimize the interference between orifices. The base was instrumented with 28 orifices, and the inserted part with 6–18 orifices, depending on the step height and length. The time-averaged measurements were taken over 2 s at a sampling rate of 5000 Hz.

III. Measured Drag Coefficient

Figure 2 shows an example of the measured surface pressure coefficient distribution for $\ell/H = 0.16$, where the variable s denotes the dimensionless distance measured from the center of the back surface of square main body along the perimeter of the stepped-nose object as shown in Fig. 1. In the measurements for $h/H = 0.16$, the pressure on the step surface takes a large negative value, implying that a net forward thrust force acts in the step regions. At the same time, the almost uniform negative pressure on the back surface of the main body together with the positive pressure on the front surface of the nose creates a net backward drag force. Frictional drag is negligible compared with pressure drag at the Reynolds number used in these experiments, and so the drag coefficient C_D was calculated by integrating the time-averaged pressure coefficient distribution shown in Fig. 2 over the perimeter (front, step, and back surfaces) of the object.

Results for all the experiments are shown in the contour plot of Fig. 3a. Because Reynolds number effects are not significant within the experimental range tested, the drag coefficient C_D is plotted as a function of step height h and length ℓ. The drag coefficient measured for the square main body of the object was $C_D = 2.26$, which is consistent with the results of previous studies [4–6]. The shaded and unshaded regions on the plot show where C_D for the stepped-nose object is greater than or less than this value, respectively. It can be seen that there exist step dimensions that reduce C_D to less than half the value for the square reference block.

For reference, two lines based on discontinuous flow theories are shown in the plot of Fig. 3a. The right-hand (dotted) line shows results for a flat-plate flow solution as shown in Fig. 3b (right). If the flat plate has the same width as the front surface of the nose of the stepped-nose object, the rest of the object, including the corners of the step base part, can be completely included within the Kirchhoff free streamlines [7], which are formed behind the plate. Therefore, to the left of this line, the stepped corners are completely within the Kirchhoff dead flow region. The left-hand (broken) line shows discontinuous flow solution results [8,9] for a semi-infinite stepped-nose body. The body extends infinitely downstream, i.e., to the right as shown in Fig. 3b (left). In this solution, the flow separates from the corners of the front face of the nose, and then reattach smoothly onto the side faces of the main body of the object at their leading edges. This represents the optimal step-flow configuration. The step regions enclosed by the step walls and the free streamlines are dead flow regions, which have a lower pressure than the uniform stream [8].

Received 20 February 2006; revision received 20 July 2006; accepted for publication 21 July 2006.

*Graduate student; currently Engineer, Riken Corporation; anangjp@ybb.ne.jp.

†Professor, Department of Aerospace Engineering; akira@nuae.nagoya-u.ac.jp.

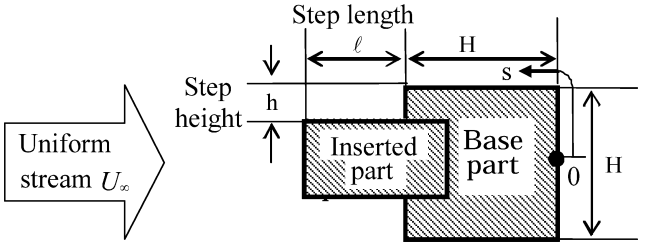

Fig. 1 Configuration of the two-dimensional stepped-nose object used in the present experiments.

Moreover, the potential flow solution to this semi-infinite object indicates that it has no net drag. It is thus natural to expect that a large drag reduction will occur in the vicinity of this line, as shown in Fig. 3a.

However, viscous effects restrict the realization of the optimal step-flow condition to a rather narrow range of step heights (h/H), but extend it to a wider range of step lengths (ℓ/H). This is because the vortex trapped in the step regions can act to adjust the separated flow streamline to reattach to the main body's side surfaces by means of the following stability mechanism: If the separated flow streamline has moved out, away from the leading edge of the main body, then the separated flow drags out some of the fluid in the step region, causing pressure in this region to decrease from the values

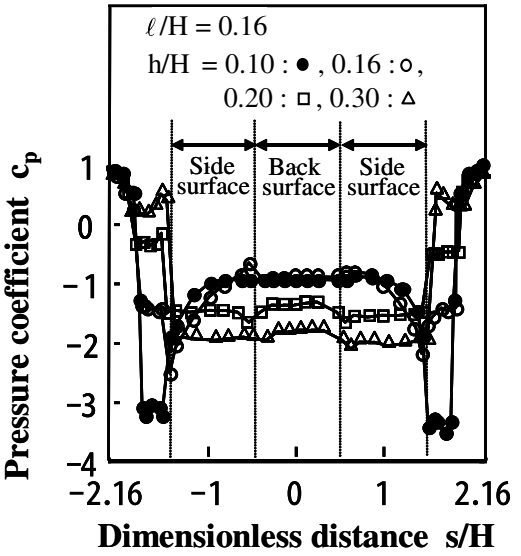

Fig. 2 Examples of surface pressure measurement results.

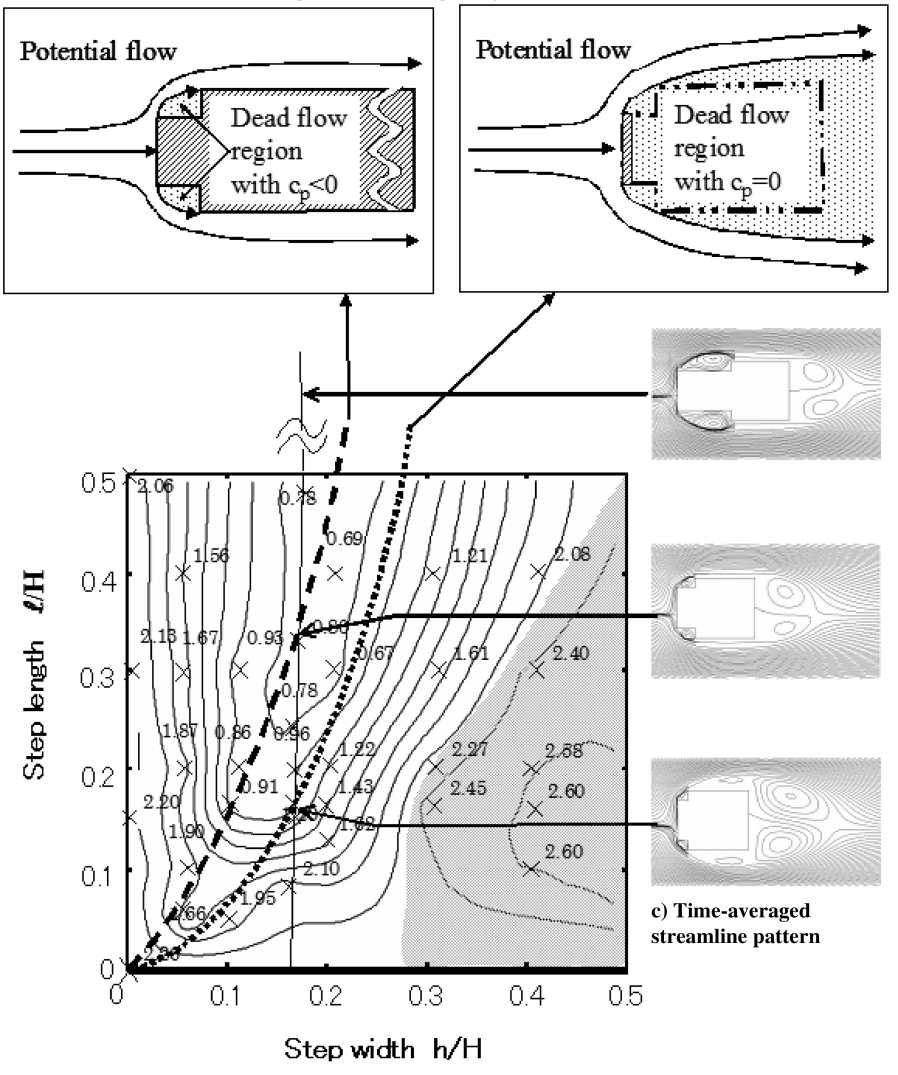

Fig. 3 Dependence of the drag coefficient on the step size.

corresponding to the optimum flow configuration as described. This has the effect of drawing the separated flow streamline back towards the leading edge of the main body, and so the flow returns to the optimum step-flow configuration. Conversely, if the flow separated from the front face of the nose impinges on the front-facing section of the step, pressure in the step region increases from the values corresponding to the optimum flow configuration, which pushes the separated flow outwards to avoid impingement, and thus, again, the flow returns to the optimum configuration.

Three time-averaged streamline patterns [9] were obtained by solving the two-dimensional Navier–Stokes equations with fractional step [10] and time splitting methods [11], and are shown in Fig. 3c. These show the change in the flow pattern with increasing step length. The mesh used had a variable grid spacing, becoming finer closer to the body to resolve the boundary layer, especially in the vicinity of the instep. A total of around 60,000 mesh points were used. The calculation was validated by comparing it to the calculated drag coefficient of a simple square ($C_D = 2.20$) and to its Strouhal number ($St = 0.15$) as reported in [5,6]. The figures were derived from the velocity field, averaged over a cycle of fluctuating drag coefficients after the calculated flow became steady. It was found that the time-averaged flow pattern approximately follows the features of the discontinuous flow obtained from the analytical solutions illustrated in Fig. 3b.

There is a lower limit to the beneficial step size. The discontinuous flow solution predicts a negatively diverging step region pressure as the step size is reduced along the broken line in Fig. 3a. This means that, if the optimal step-flow configuration is realized for a small step size, the side flow is exposed to a large adverse pressure gradient. The resulting side flow separation leads to the same magnitude of drag coefficient as for the square body case. This is why the drag coefficient in the vicinity of the origin in Fig. 3a takes the same value as for the square. Because the drag coefficient of a rectangular object ($h = 0$) decreases with its length, Fig. 3a suggests that the drag reduction effect from the stepped corner, identifiable with the difference $C_D(h = 0, \ell) - C_D(h, \ell)$, is a maximum for a step of dimensions around $h/H = 0.1$ and $\ell/H = 0.16$.

IV. Conclusions

In the present study, we measured the surface pressure distribution on stepped objects to determine the optimal step size for drag reduction. An important characteristic of the optimal step size is the large pressure drop inside the vortex trapped in the step region, which effectively suppresses large-scale flow separation and significantly reduces the drag coefficient. The effects of step size on drag agree with calculations using discontinuous flow theory. However, the presence of viscosity restricts the realization of optimal step-flow to a rather narrow range of step heights h, but extends it to a wider range of step lengths ℓ, because the vortices trapped in the step regions can act to adjust the separated flow to reattach at the leading edges of the main body's side surfaces.

References

[1] Koenig, K., and Roshko, A., "An Experimental Study of Geometrical Effects on the Drag and Flow Field of Two Bluff Bodies Separated by a Gap," *Journal of Fluid Mechanics*, Vol. 156, July 1985, pp. 167–204.

[2] Watanabe, K., "Characteristics of Axial Flow Around Step Cylinder (Parallel Flow)," *Transactions of the Japan Society of Mechanical Engineers, Series B*, Vol. 62, April 1996, pp. 2130–2136.

[3] Ruderich, R., and Fernholz, H. H., "An Experimental Investigation of a Turbulent Shear Flow with Separation, Reverse Flow and Reattachment," *Journal of Fluid Mechanics*, Vol. 163, Feb. 1986, pp. 283–322.

[4] Lyn, D. A., Einav, S., Rodi, W., and Park, J. H., "A Laser-Doppler Velocimetry Study of Ensemble-Averaged Characteristics of the Turbulent Near Wake of a Square Cylinder," *Journal of Fluid Mechanics*, Vol. 304, Dec. 1995, pp. 285–320.

[5] Taylor, I., and Vezza, M., "Prediction of Unsteady Flow Around Square and Rectangular Section Cylinders Using a Discrete Vortex Method," *Journal of Wind Engineering and Industrial Aerodynamics*, Vol. 82, Aug. 1999, pp. 247–269.

[6] Taylor, I., and Vezza, M., "Calculation of the Flow Field Around a Square Section Cylinder Undergoing Forced Transverse Oscillations Using a Discrete Vortex Method," *Journal of Wind Engineering and Industrial Aerodynamics*, Vol. 82, Aug. 1999, pp. 271–291.

[7] Imai, I., *Fluid Dynamics*, Shyokabo, Tokyo, 1977, pp. 237–258.

[8] Roshko, A., "On the Wake and Drag of Bluff Bodies," *Journal of the Aerospace Sciences*, Vol. 22, Feb. 1955, pp. 124–133.

[9] Cakrawala, A., "Experimental Investigation on Aerodyanimc Characteristics of Stepped-Nose Obstacles," Ph.D. Dissertation, Dept. of Aerospace Engineering, Nagoya Univ., Nagoya, Japan, 2006.

[10] Harlow, F. H., and Welch, J. E., "Numerical Calculation of Time-Dependent Viscous Incompressible Flow of Fluids with Free Surface," *Physics of Fluids*, Vol. 8, Dec. 1965, pp. 2182–2189.

[11] Chorin, A. J., "Numerical Solution of the Navier-Stokes Equations," *Mathematics of Computation*, Vol. 22, Oct. 1968, pp. 745–762.

N. Chokani
Associate Editor